The International Journal of
Robotics Research
30(1) 118–133

DOI: 10.1177/0278364910382862
ijr.sagepub.com

Waalbot II: Adhesion Recovery and Improved Performance of a Climbing Robot using Fibrillar Adhesives

Michael P. Murphy, Casey Kute, Yiğit Mengüç and Metin Sitti

Abstract

This paper presents the design and optimization of a wall-climbing robot along with the incorporation of autonomous adhesion recovery and a motion planning implementation. The result is Waalbot II, an untethered 85 g robot able to climb on smooth vertical surfaces with up to a 100 g payload (117% body mass) or, when unburdened, on planar surfaces of any orientation at speeds up to 5 cm/s. Bio-inspired climbing mechanisms, such as Waalbot II's gecko-like fibrillar adhesives, passive peeling, and force sensing, improve the overall climbing capabilities compared with initial versions, resulting in the ability to climb on non-smooth surfaces as well as on inverted smooth surfaces. Robot length scale optimization reveals and quantifies trends in the theoretical factor of safety and payload carrying capabilities. Autonomous adhesion recovery behavior provides additional climbing robustness without additional mechanical complexity to mitigate degradation and contamination. An implementation of a motion planner, designed to take into account Waalbot II's kinematic constraints, results in the ability to navigate to a goal in complex three-dimensional environments while properly planning plane-to-plane transitions and avoiding obstacles. Experiments verified the improved climbing capabilities of Waalbot II as well as its novel semi-autonomous adhesion recovery behavior and motion planning.

Keywords

Climbing robots, adhesion recovery, fiber adhesives, gecko

1. Introduction

Animal mobility far exceeds the capabilities of mobile robots in terms of agility, robustness, and terrain flexibility. Climbing animals are able to navigate complex, unstructured three-dimensional (3D) environments while scaling a wide variety of surfaces, such as trees, rocks, and in the case of geckos and many insects, smooth vertical and inverted surfaces. The gecko is able to climb on smooth surfaces by exploiting surface contact forces, such as van der Waal's forces, between small hair-like structures on the feet and the climbing surface (Autumn et al. 2000). In addition to demonstrating advanced agility capabilities, geckos have been shown to utilize their tails as an emergency fifth leg to prevent falling after sensing a loss of adhesion (Jusufi et al. 2008). Similar emergency behaviors are common among climbing animals, as the consequences of a fall can be deadly. Recent advances in robot mobility have resulted in climbing robots that scale vertical surfaces using various attachment mechanisms. A similar sensing and recovery mechanism to that of the animal tail for climbing robots could prove useful to prevent unwanted detachment from climbing surfaces.

In addition to climbing robots using attachment mechanisms such as grasping with claws, spines, or grippers (Bretl et al. 2003; Kim et al. 2005; Linder et al. 2005; Guan et al. 2007; Daltorio et al. 2009), magnetic clamping (Grieco et al. 1998; Shen et al. 2005; Fei et al. 2006; Kalra et al. 2006; Berengueres et al. 2007), pressure differential by suction cups (Hirose et al. 1991; Ryu et al. 2001; Lal Tummala et al. 2002; Cacopardo et al. 2003; Kim et al. 2006; Wu et al. 2006; Zhu et al. 2006; Wang et al. 2008; Wanli et al. 2007) or scanning suction cups (Yano et al. 1997; Yan et al. 1999; Miyake and Ishihara 2003; yuan Qian et al. 2006; Saboori et al. 2007; Xiao and Sadegh 2007), and electroadhesion (Yamamoto et al. 2007; Prahlad et al. 2008), synthetic dry fibrillar adhesives are starting to be utilized as attachment mechanisms for biologically

NanoRobotics Laboratory, Department of Mechanical Engineering, Carnegie Mellon University, Pittsburgh, USA.

Corresponding author:
Metin Sitti
NanoRobotics Laboratory, Department of Mechanical Engineering
Carnegie Mellon University, Pittsburgh, PA 15213-3890, USA.
Email: sitti@cmu.edu.

inspired climbing robots. Recent advances in synthetic fibrillar adhesive technology, such as high adhesion from carbon nanotube arrays (Yurdumakan et al. 2005; Zhao et al. 2006; Ge et al. 2007; Sethi et al. 2008; Qu et al. 2008), geometric fiber tip control (Bhushan and Sayer 2006; Kim and Sitti 2006; delCampo et al. 2007; Murphy et al. 2007), directional adhesion (Santos et al. 2007; Lee et al. 2008; Jeong et al. 2009; Murphy et al. 2009a), and hierarchical structures (Jeong et al. 2009; Murphy et al. 2009b), have increased the performance of these materials to the point where they can be successfully implemented as attachment mechanisms in climbing robots. Daltorio et al. (2009) outfitted their Mini Whegs robot with mushroom tipped synthetic dry adhesives and demonstrated climbing smooth vertical glass. Similarly, Kim et al. (2008) constructed a legged robot resembling a gecko, which uses directional polymer adhesives to climb up smooth surfaces. Then, Santos et al. (2008) showed climbing on slightly underhanging surfaces and Asbeck et al. (2009) showed successful climbing on rough surfaces using hierarchical adhesives.

Waalbot II (Figure 1), named after the van der Waal's forces it dominantly uses to climb, is a small-scale agile wall climbing robot able to climb on planar surfaces of any orientation using flat adhesive elastomers or fibrillar adhesives for attachment (Murphy and Sitti 2007). The essential morphology and force transfer concept of the Waalbot design was first seen in a robot created by iRobot, named Mecho-Gecko, which had a tri-leg design that was used to passively peel pressure sensitive adhesives off the climbing surface while climbing (Autumn et al. 2006). However, Waalbot II uses flat or fibrillar elastomer adhesives as the attachment material and has steering and surface transitioning abilities. Using two actuated legs with rotary motion and two passive revolute joints at each foot, this robot can climb and steer in any orientation (Figure 2). The passive revolute ankle joints allow the feet to pivot forward to remain in contact with the surface during stepping (Figure 3). An elastic band is used to passively return the foot to the forward position after each step. Due to the minimalistic and compact design, a high degree of miniaturization is possible. The robot carries on-board power, a printed circuit board (PCB) for computing, and an infrared (IR) receiver or radio frequency (RF) transceiver for wireless communication, which allows for semi-autonomous operation. The average power consumption for Waalbot is 2.4 W for an average vertical climbing speed of ∼5 cm/s (0.5 body lengths/s). Waalbot climbs using synthetic fibrillar adhesives or a pressure sensitive dry adhesive elastomer and is also able to make sharp turns (Murphy and Sitti 2007) and plane transitions, including floor-to-wall, wall-to-wall, and wall-to-ceiling transitions. The robot is also intended to climb real-world surfaces that are not completely smooth, such as a painted wall or wood surface.

Waalbot was first introduced by Murphy and Sitti (2007) using flat elastomers to climb. The improvements presented in this work build upon the basic design principles of the robot to increase capabilities (refer to Table 1 for major improvements). One major change was the utilization of dry fibrillar gecko-inspired adhesives onto Waalbot II, initially introduced in Aksak et al. (2008), with further testing and performance improvements presented in this paper. Since the adhesion ability of the footpads increased due to the fibrillar adhesives' performance, a better passive peeling mechanism was implemented to increase reliability and mobility. Waalbot II is now equipped with force sensors that allow for monitoring of the adhesive's performance. Waalbot II, while climbing, autonomously performs actions to regain adhesion and prevent detachment from climbing surfaces, an action inspired by animals that use sensory feedback to determine adhesion strength and prevent detachment by changing their climbing gaits when adhesion is low (Jusufi et al. 2008). The chassis design of the robot was also changed to include two tails for stability and surface adaptation while climbing. Waalbot II also follows paths as generated by a motion planner to traverse complex 3D environments.

In this paper, Section 2 describes the implementation of improved climbing mechanisms, including fibrillar adhesives and passive peeling, force transfer discussions, and details on the capabilities and performance of Waalbot II. Length scale optimization is explored in Section 3. Waalbot II's ability to regain adhesion lost while climbing due to fiber degradation is discussed in Section 4. Implementation details and specifications for a motion planner to aid in the exploratory climbing abilities of Waalbot II are also discussed in Section 4. Finally, conclusions and future directions are reported in Section 5.

2. Waalbot II Design Improvements

In this section, we explore the force analysis for Waalbot II to provide a set of guidelines used in the physical design of the robot. Next, the details of the physical changes to the robot from Murphy and Sitti (2007) are explained, which include the synthetic adhesive fiber integration, modification to the tail, and the peeling mechanism. Finally, the capabilities are discussed and the performance of Waalbot II is demonstrated.

2.1. Footpad Size Design

Each of Waalbot II's legs have three feet. When the legs rotate, the forward foot contacts the surface, while the rear foot is peeled from the surface (Figure 3). For a particular footpad adhesive material, climbing surface, and actuator, there is a limit to the amount of footpad area the actuator can pull off from the wall. The pull-off direction during stepping is normal to the climbing surface, whereas the footpads are designed to support the robot's weight irrespective of the loading direction.

Examining a free body diagram of the Waalbot II foot in the highest loading configuration during stepping, we find the equations to use to optimize the footpad design. Figure 4 illustrates the footpad adhered to a surface at an angle

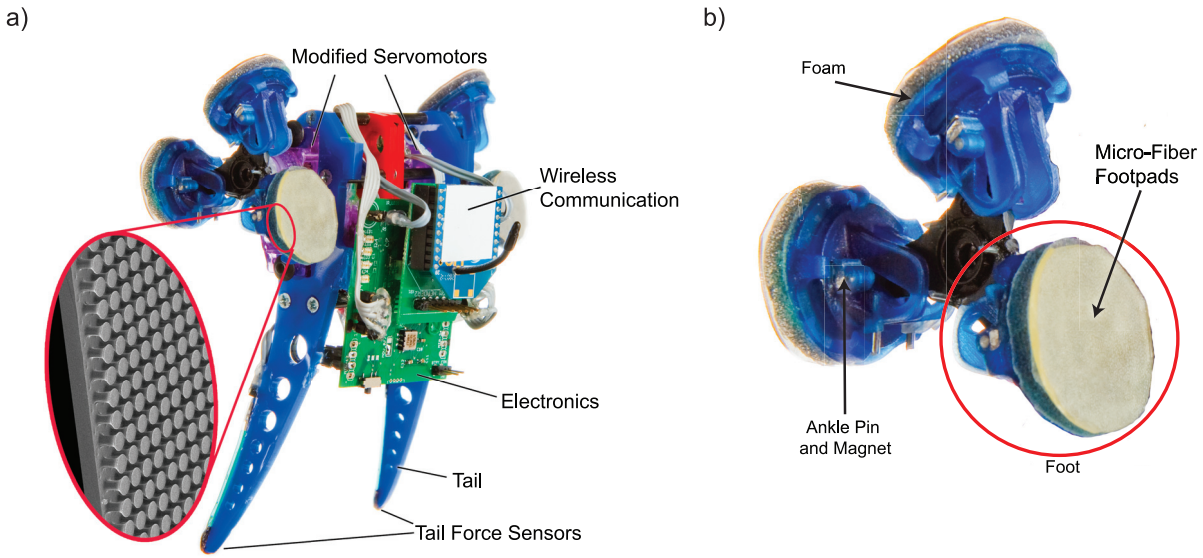

Fig. 1. (a) Photograph of Waalbot with components labeled and an inset of a scanning electron microscope image of the gecko-inspired dry fibrillar adhesives used in the footpads. (b) Details on naming conventions used for the leg and its components.

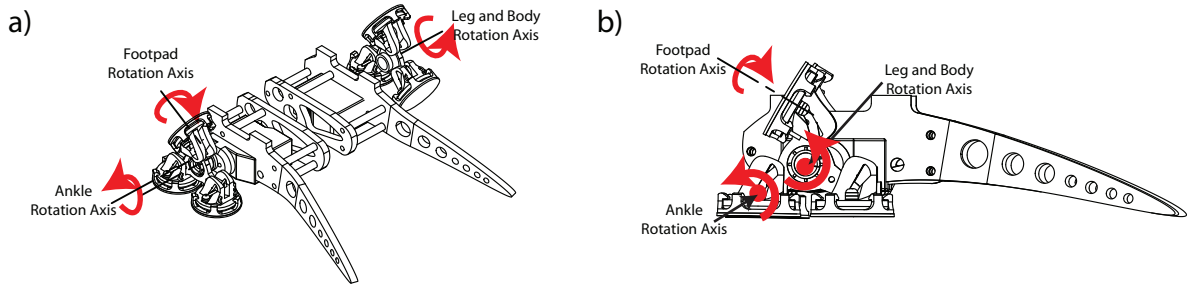

Fig. 2. Computer-aided design (CAD) diagrams showing the axes of rotation: (a) partially exploded view to see the separation between the two sides and between the servo horn and the legs; (b) side view showing three axes of rotation.

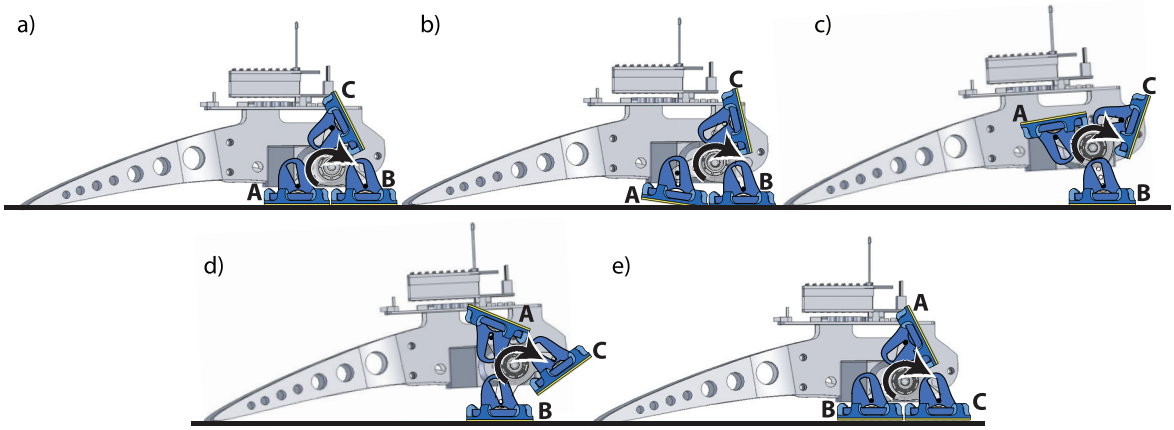

Fig. 3. CAD diagrams showing the stepping process for a forward step (leg rotating clockwise in image). (a) Two feet (**A** and **B**) are in contact; (b) foot **A** is peeled from the surface; (c) foot **A** releases from the surface and the robot begins to move forward; (d) foot **C** rotates closer to make contact with the surface; (e) foot **C** achieves contact with the surface and now foot **B** is the rear foot. The process continually repeats for forward movement.

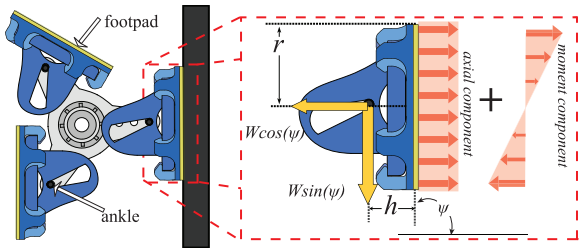

Fig. 4. Free body diagram of one of Waalbot II's feet adhered to a surface of angle ψ. The distributed stresses on the footpad consist of the axial component and the moment component.

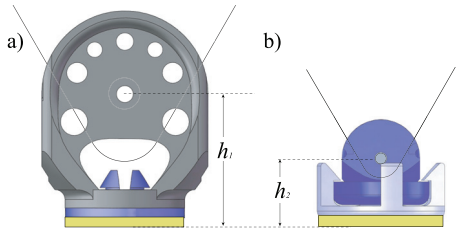

Fig. 5. Moving the footpad attachment tabs from the center of the footpad (a) to the perimeter (b) allows the ankle joint to be placed closer to the climbing surface, reducing the peeling moment.

ψ with respect to the ground. Load W is acting on the pin ankle joint, which is at a distance h from the climbing surface. Instead of considering only point forces, we can assume distributed loading across the footpad. Solving for the maximum stress, $\sigma_{\max}$, which occurs at the top edge of the footpad in this case, yields

$$\sigma_{\max} = \frac{W \sin(\psi)\, h}{I} + \frac{W \cos(\psi)}{A} \qquad (1)$$

where I is the second moment of area of the footpad cross-section, and A is the area of the footpad. The first term in (1) results from the peeling moment, while the second term is the stress caused by the axial loading (loading in the direction normal to the surface). The maximum footpad area A is determined by the adhesive–surface interaction, and actuator. The load W is determined by the weight of the robot and geometric parameters. The remaining design parameters that can affect the maximum stress are the height from the surface to the ankle joint (h), and the second moment of area. To reduce the component of the maximum stress due to the moment, which will yield better robot performance, it is important to design the ankle such that the distance h is as small as possible, and I is as large as possible. The design of the passive revolute joint at the footpad, which allows for better robot agility, has been changed to decrease h by changing the footpad revolute joint from a rotation joint in the center to tabs around the perimeter. The tabs rigidly attach the footpad to the foot so as to not allow translation, but slide to allow footpad rotation. Moving this joint allowed the ankle joint to be lowered because the footpad attachment tabs were no longer in conflict with the leg, which reduced the peeling moment during climbing. The change in h as a result of this design change can be seen in Figure 5.

2.2. Tail Design

The adhesives are optimally useful when correctly aligned to the climbing surface. Waalbot II has been redesigned to have two passive tails, each with the contact point aligned directly behind the feet on that side. A passive rotation joint connects the two sides of the robot, aligned with the center of rotation of the legs. The two sides can pivot relative to each other (Figure 6(d)), allowing each side to rotate independently. During tests of fixed body prototypes (Figure 6(a)), the robots often fell from the wall, twisting laterally as they came off of the surface. It was determined that poor synchronization was causing the feet to detach from each side at slightly different times. When one foot pulls off before the other, a lateral force imbalance (Figure 6(c)) is formed across the robot, and the resulting torque peels one side of the robot from the wall. In the current design, with the tails aligned with the feet, these plane forces are not transferred to the opposite side. This allows the robot to act more like the simplified two-dimensional (2D) model detailed in previous work (Murphy and Sitti 2007). Performance indicates that this design is a significant improvement over the rigid, single-tail design.

2.3. Fiber Footpad Implementation

For very rough surfaces, such as brick, gripping with claws has been demonstrated to be an effective method (Haynes and Rizzi 2006; Kim et al. 2005), and for smooth glass-like surfaces, adhesive attachment mechanisms have been successfully implemented (Daltorio et al. 2009; Kim et al. 2008). However, many surfaces do not fall into either of these two categories (very rough or very smooth). Previous Waalbot prototypes were able to adhere to smooth flat surfaces using flat unstructured adhesive elastomer pads. However, when placed onto a non-smooth climbing surface, such as a painted wall or wooden door, the flat adhesives do not support the robot, even in the static case. To climb these slightly rough surfaces, gecko-inspired fibrillar adhesive footpads were used, which we have shown to have superior adhesion to non-smooth surfaces in microscale studies (Aksak et al. 2008).

Polyurethane fibrillar footpads were fabricated as described previously in Aksak et al. (2007) and Murphy et al. (2007), using ST-1060 (BJB Enterprises) with a shore hardness of 60 A, and a Young's modulus of approximately 2.4 MPa. The fibers had dimensions of 57 μm stem diameter, 114 μm tip diameter, and 113 μm length as seen in Figure 1(a). The center-to-center spacing between the square packed fibers was either 80 or 120 μm. These arrays were cut into the circular footpad shape with 19 mm diameter.

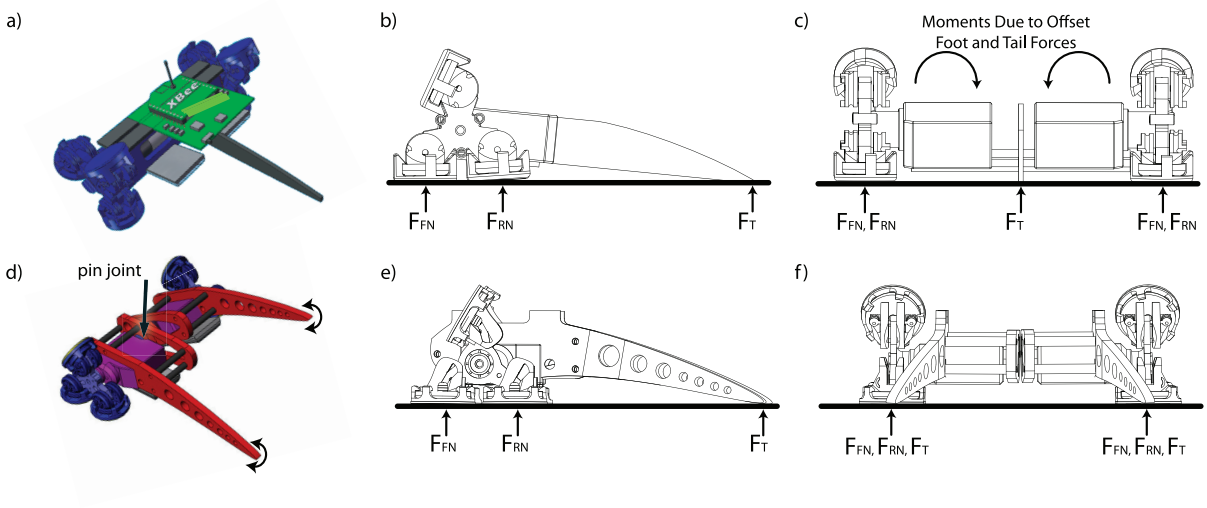

Fig. 6. (a) CAD model of the previous Waalbot prototype showing the rigid body, fixed tail design. Partial free body diagrams showing the forces present during a forward step. F_{RN} and F_{FN} are the rear and front forces, respectively, in the direction normal to the surface, while F_T is the tail force. (b) Side view of single tail design. (c) Rear view of single tail design showing the coupling moments between the two sides of the robot. (d) CAD model of the new Waalbot II prototype outlining the passive rotation joint between the two sides of the robot allows each side to *rotate* independently to prevent torque transfer between the feet on opposite sides. (e) Side view of the two tail design. (f) Rear view showing the alignment of the each tail with the footpads on each side of the two tail robot design.

The footpads are attached to the robot with a thin layer, 2.8 mm, of soft foam, with a stiffness of 676 N/m, between the foot and the fibrillar adhesive pad. This foam adds large-scale compliance to the footpad, which decreases the likelihood of misalignment between the fibers and climbing surface, and increases load uniformity over the pad area during preloading (Unver and Sitti 2009). This increases the total number of fibers that are pressed into contact with the surface and prevents small areas from absorbing all of the preload force. As a demonstration of the application of the fibrillar adhesives on Waalbot II, the robot (mass = 85 g) climbed up a vertical wooden cabinet door (Figure 7(a)) with a high surface roughness (35 μm root mean square (RMS) roughness and 120 μm peak-to-peak height). This surface roughness was high enough to prevent the robot from sticking to the surface at all with flat unstructured adhesive pads. Aksak et al. (2008) analyzed the fibrillar adhesives conformation to surface roughnesses and showed that a higher effective contact area is obtained with the fibrillar adhesives than with flat tacky elastomers, as was initially used on Waalbot, and they therefore exhibit higher adhesion performance. Using the fibrillar footpads, the robot was able to climb over 30 steps before detaching from the surface (Figure 7(a)). In subsequent attempts with the same footpads, the robot took successively fewer steps each time before falling, and eventually was unable to adhere to the surfaces at all. Contamination of the fibers was observed by eye and optical microscopy after Waalbot was unable to adhere sufficiently to the wooden cabinet door, which suggests that contamination was the cause of the severe adhesion degradation. Gecko feet are self-cleaning (Hansen and Autumn 2005) and incorporation of this ability for the synthetic fibrillar adhesives is currently ongoing.

2.4. Passive Peeling to Prevent Immobilization

After integration of the fibrillar footpads, the most significant issue with Waalbot II was footpad adhesion consistency. It was difficult to achieve the correct balance between safety and over-adhesion. If even one of the footpads does not adhere with enough strength, the robot may detach from the wall – an unacceptable result for a climbing robot. Therefore, there is motivation to include in the design a large margin of safety. On the other hand, if any of the footpads has adhesion that is too strong, the robot can become immobilized when the actuator cannot provide sufficient torque to detach the foot, or worse, the torque provided by the actuator is high enough to cause a mechanical failure of parts of the robot.

This issue is compounded when the desired climbing surfaces are made of varied materials. While it is possible to tailor footpads so that the adhesion properties match the desired climbing surface, this does not allow the robot to climb on different surfaces using one set of legs. For example, a set of legs that climb well on wood may provide excessive adhesion to glass. Furthermore, as the robot climbs on surfaces, the footpads can degrade by picking up dust and dirt. The reality of degradation by contamination, as well as the objective of climbing on more than one surface with the same footpads, creates a very small and sometimes nonexistent parametric space for the adhesion properties of the footpads.

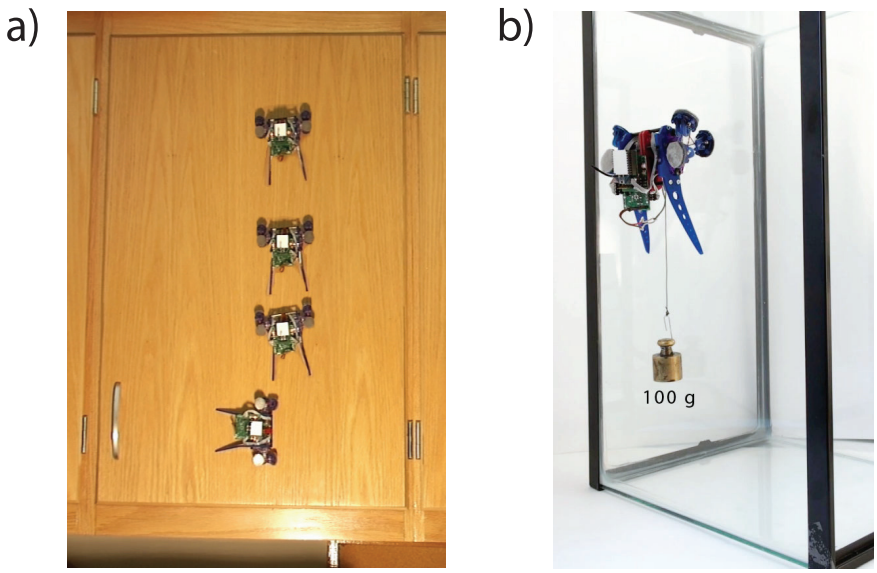

Fig. 7. (a) Composite still frames of a video showing Waalbot II climbing a rough wood vertical cabinet. (b) Still image from a video frame illustrating the climbing payload capacity of Waalbot on smooth vertical surfaces.

Luckily, nature has demonstrated a solution to this issue. Many animals that use dry adhesion to climb, including geckos, detach their pads by peeling. Peeling requires much smaller forces than pulling off in the normal direction because only small sections of the fibers are loaded at a time instead of loading all of the fibers at once. Designing a mechanism that enables the robot to switch to peeling mode to detach the footpads once the landing feet are firmly pressed onto the surface, or preloaded, allows the use of much stronger dry adhesives, or larger adhesive areas. Peeling effectively raises or, ideally, removes the upper bound on adhesion constraints, and the goal becomes the creation of the strongest dry fibrillar adhesive possible. In this case, the steady-state operating adhesion and margin of safety can be increased, improving the robustness of adhesion, even on smooth surfaces, without increasing the motor torque requirements.

Other wall-climbing robots successfully use peeling to reduce detachment forces. Geckobot uses compliant footpads which peel passively (Unver et al. 2005, 2006), and Stickybot uses active toes to peel away from climbing surfaces (Kim et al. 2008). These designs are effective in reducing problems with foot detachment. However, Waalbot II's design utilizes the detachment forces to preload the front feet, so a different approach must be taken to detach its feet while ensuring high preload forces.

To implement such a peeling design into Waalbot II, while maintaining the minimalistic, scalable design of the robot, a passive design was chosen over an actuated approach. The added weight and power consumption of actuators, along with the complications of actuating six distal feet on a rotating joint, were avoided by implementing a self-peeling ankle design. In previous designs, the ankle axle was fixed in place at all times. During the preloading and detachment phases of a step, the force is transmitted through the axle in the normal direction, evenly stressing the rear footpads. This detachment method is effective in creating large preload forces on the front feet. However, once a sufficient preload is reached, it is no longer necessary for the rear feet to resist detachment. In the self-peeling design, permanent magnets hold the axle in its home position until the desired preload is reached. This preload threshold value is set by the holding strength of the magnets. If the feet detach from the climbing surface without reaching the threshold force, the ankles act identically to the previous designs (Figures 8(a) and (c)). However, if the threshold force is reached before detachment, the magnets are pulled from each other and the rear ankle's axle begins to move within the ankle slot (Figures 8(b) and (d)), attempting to follow the arc shown in Figure 8(a). As the axle slides, the force vector on the ankle is rotated to be normal to the contact between the axle and the slot (Figure 8(b)). The change in direction of the force causes the footpad to be asymmetrically loaded, resulting in peeling from the posterior edge forward as seen in Figure 8(d). Since the footpad is rigid, this is not true peeling as seen in the gecko's toes.

To test the effectiveness of the peeling mechanism, a single Waalbot II servo was mounted above a 10 lb load cell (MLP-10; Transducer Techniques Inc.). A leg was attached to the servo and the footpad adhesive foam was preloaded to an acrylic surface, which was connected to the load cell (Figure 9). The servo then rotated forward, as if taking a step, and the force over time was monitored for the

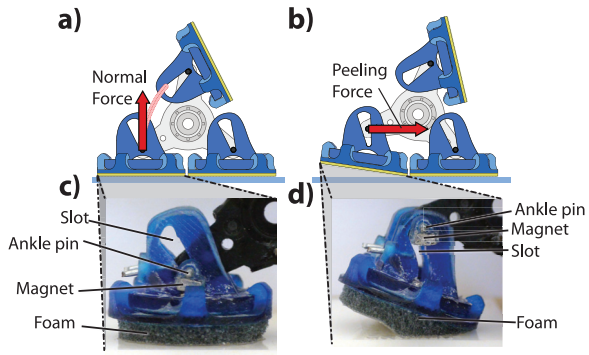

Fig. 8. Illustration and photographs of the passively peeling ankle mechanism. (a) The peeling force is normal to the surface during the preloading phase. (b) After a threshold force is reached, the axle moves freely up a slot in the ankle, and the force vector rotates. The new direction of the peeling force causes the foot to peel from the posterior edge. (c) An image of the locked axle showing uniform loading across the foam adhesive. (d) An image of the peeling mechanism showing asymmetric loading, which causes the foam to peel from the posterior edge.

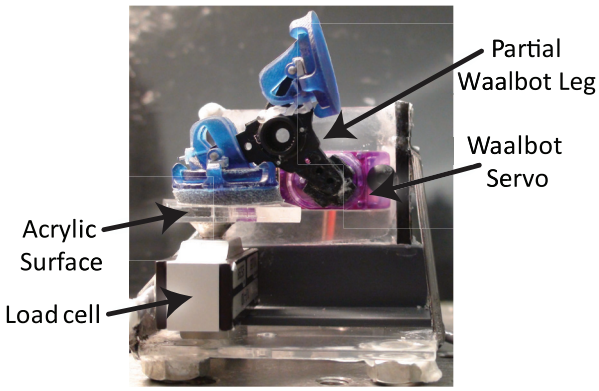

Fig. 9. Experimental setup for pulling off foam adhesive footpads using locked (normal force, no peeling) and unlocked (peeling) ankle axles.

cases when the axle was glued in place so as to never allow for a change in the direction of the pull-off force and when the axle was free to move after the magnet threshold was exceeded. The motor current was measured across a sense resistor using a data acquisition board (NI PCI-6259; National Instruments). The passive peeling design requires the motors to use less power to peel the adhesive (Figure 10(b)). As seen in Figure 10(a), the peeling mechanism also greatly decreases the amount of time required to detach the foot and thus allows the robot to climb faster.

2.5. Capabilities and Performance

While carrying power, computing, and communications devices on-board, Waalbot II has demonstrated climbing and steering abilities on vertical surfaces, including glass, acrylic, and wood, using gecko-inspired fibrillar adhesives. On smooth surfaces, climbing in any direction on vertical surfaces has been demonstrated. Waalbot II has also demonstrated floor-to-wall (Figures 11(a)–(c)), wall-to-wall (Figures 11(d)–(e)), and wall-to-ceiling (Figures 11(f)–(h)) transitions consecutively inside a smooth acrylic enclosure, steering on each plane to align for the subsequent transitions. Transitions, particularly wall-to-ceiling transitions, were found to be frequently unsuccessful due to interactions between the approaching feet and the transition corner. To mitigate this problem, the robot must approach the transition perpendicularly and additional compliance in the foot design could ease this constraint. Climbing and turning on smooth inverted surfaces, such as the ceiling of an acrylic enclosure, has also been demonstrated. However, the robot can be unsuccessful in climbing safely when the adhesives degrade or a misstep is taken which does not allow the foot to be properly preloaded to yield a sufficient adhesion (Figure 12). Waalbot II is capable of carrying a payload of up to 100 g, or 117% of its body weight, when climbing a smooth vertical surface as illustrated in Figure 7(b). High payloads decrease the reliability of the robot. Videos of these performances can be seen in Extension 1.

3. Length Scale Optimization

The same physical laws govern the behaviors of animals and robots of vastly varying sizes, but different forces tend to dominate at different scales. In climbing robots and animals the two most important parameters are the total adhesive area and mass, and these parameters scale differently. Given constant geometric proportions, as a climbing robot's length scale increases monotonically, its foot area increases as the square of the length and its mass increases as the cube of the length. This carries a very strong implication: a climbing robot that is doubled in size will have four times as much adhesion but eight times as much mass and hence its adhesion to weight ratio will have been halved. In this section we develop an optimization model to help determine the appropriate size scale for a given payload requirement.

In developing the optimization analysis certain constants and relationships were assumed. First, the robot's geometric proportions stay constant as its size varies (isometric scaling). Additionally, a constant small mass of 10 g, for all robots, was included as the weight of the electronics and sensors. Another constraint was applied to the maximum available adhesion by limiting the adhesion to the amount that could be pulled off by servos in the weight class related to the length scale.

The objective function of the optimization was the theoretical factor of safety of the climbing robot's adhesion, and the independent variable was the length of the robot, which was defined as the distance between the servo axle and the tip of the tail. The theoretical factor of safety is the proportion of available adhesion to the mass of the robot, meaning that a theoretical factor of safety of one represents a marginal design and less than one represents a robot that

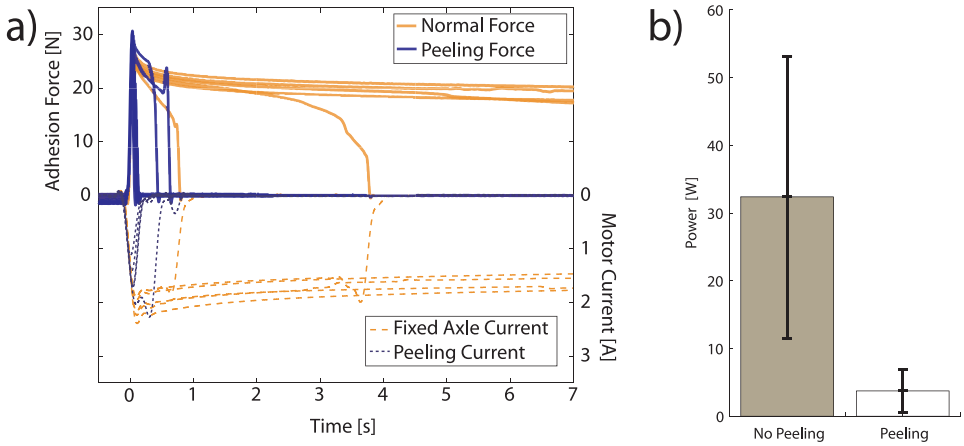

Fig. 10. Experimental data for pulling off foam adhesive footpads using locked (normal force, no peeling) and unlocked (peeling) ankle axles. (a) Force (top half of graph) and current (bottom half of graph) required to remove the foam adhesive from an acrylic surface. (b) Amount of electrical power required to remove the foam adhesive (only the locked tests where the foam was fully removed from the surface, two runs, were accounted for in the calculation).

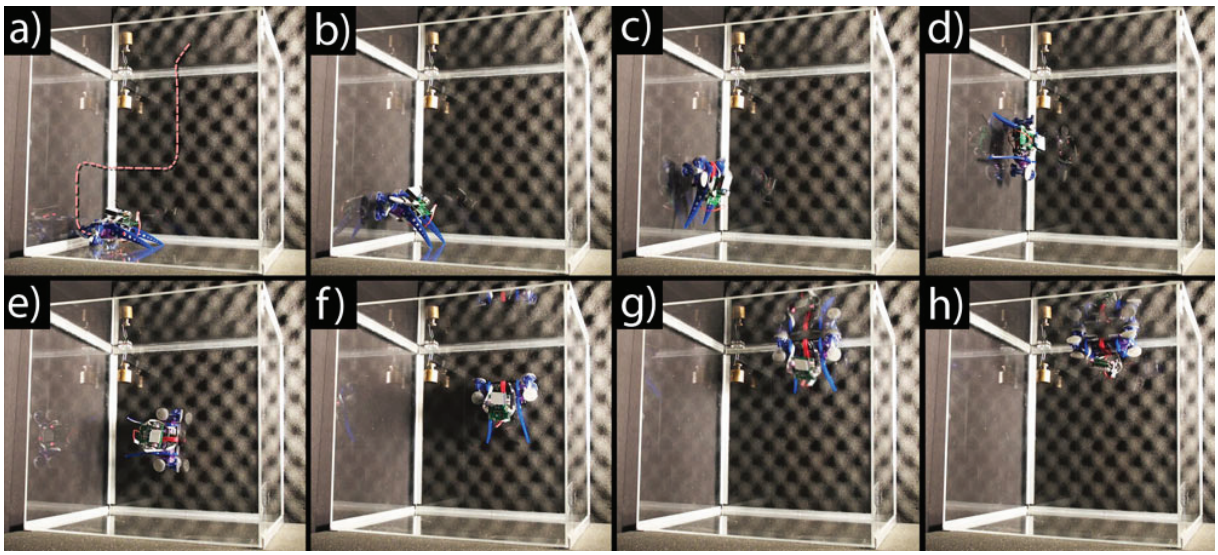

Fig. 11. Still image frames from a video of the robot climbing from the floor (a) to the wall (b)–(d), transferring to the rear wall (e),(f), and then transferring to the ceiling (g),(h) of an acrylic cube. The robot path is illustrated in (a) with an overlay. A weight is hung in the top corner for reference to show that the direction of gravity is down.

cannot climb. The primary purpose of climbing robots is to carry out some task, which requires carrying additional equipment, such as cameras, surfaces inspection sensors, and wireless communications hardware, so the optimization plots the theoretical factor of safety in relation to the length scale for varying payloads (Figure 13). The theoretical factor of safety values emerging from the optimization are artificially large because the analysis assumes ideal contact and no dynamic forces.

The optimization suggests that a larger robot will be able to carry more payload but with a smaller theoretical factor of safety, and in fact this has been observed with two different scales of Waalbot prototypes. The larger version, Waalbot II (Figure 1), with a length of 95.6 mm, can climb vertically and carry up to 100 g payloads, but has difficulty robustly climbing on ceilings. The smaller version (Figure 14), with a length of 56.1 mm, is able to climb and transition easily at all surface orientations, but requires power and electronics to be off-board and also has the problem of twisting off from the wall due to the single tail design, as described in Section 2.2. Video snapshots of the small prototype climbing inside an acrylic cube in Figure 14 illustrate the prototype consecutively climbing down a wall (a), transitioning from the wall to the floor (b), crawling across the floor (c), performing a floor-to-wall transition (d), climbing a vertical wall (e), transitioning from wall-to-wall (f),

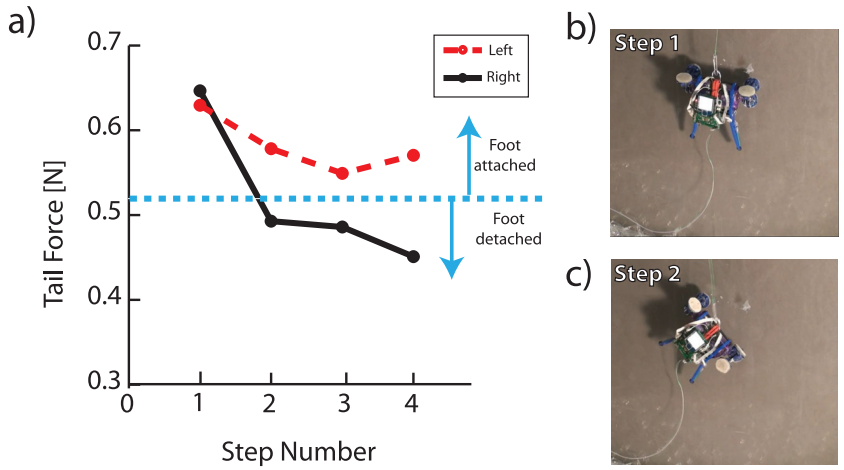

Fig. 12. (a) Plot showing force data from the two tail force sensors while the robot climbs on a smooth, vertical surface. (b) The robot starts out with sufficient adhesion to maintain attachment. (c) On the second step, the right side loses adhesion and detaches from the wall. The robot continues moving sideways, stepping with both feet, but only the left-hand side has sufficient adhesion and the right-hand side continues to slip.

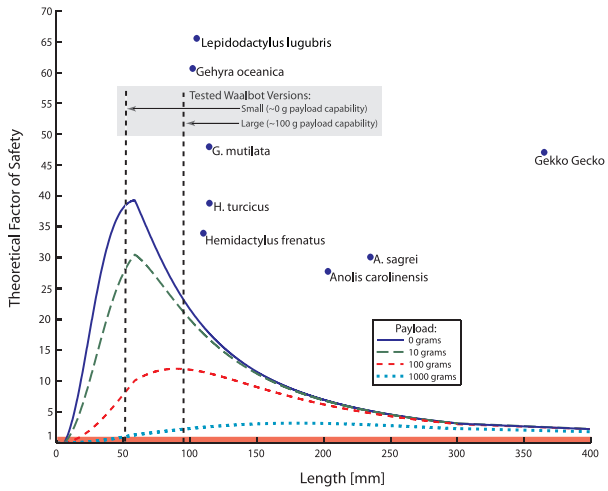

Fig. 13. Simulated length scale effect on a climbing robot's theoretical factor of safety. With increasing payload masses, the optimum size of a Waalbot increases. The shaded region along the bottom is where the theoretical factor of safety is below 1. The dots represent the calculated factor of safety for various types of pad-bearing lizards as adapted from Irschick et al. (1996).

steering on a wall (g), transitioning from the wall to the ceiling (h), performing inverted steering (i), and successfully climbing while inverted (j). These agility demonstrations indicated that both scales have good performance and can achieve the performance objectives outlined in the introduction. To increase the performance of the smaller scaled robot, the two tail design should be implemented to mitigate any synchronization problems.

The results of the scaling analysis indicate that carrying large payloads ($>$ 500 g) is not easily accomplished with this design at any scale, as indicated by the relatively low factors of safety seen in Figure 13 for the 1,000 g line. The low factor of safety indicated at larger size scales is compounded by the increasing difficulty of achieving ideal contact with the climbing surface when using larger footpads. One possible solution is to utilize several Waalbots as a team to split up the required payload, or to work together as a team to carry more massive payloads. Coordinated teams of climbing robots is a topic of interest for future work.

4. Advancements for Semi-autonomous Control

In order to move towards the development of an autonomous climbing robot, certain issues facing the current Waalbot II design were addressed. By using dry fibrillar adhesives and passive peeling, Waalbot II can climb on a variety of surfaces. However, different surface conditions and the degradation of the adhesive forces can lead to catastrophic failure. To address these limitations, Waalbot II exploits the force transfer design, by means of a rocking maneuver, to regain adhesion when a loss of adhesion is detected. Additionally, Waalbot II has kinematic constraints, such as its inability to step backwards and side step, that require foresight in climbing so that it does not get stuck. To help Waalbot II navigate its environment safely, a motion planner that takes into consideration the robot's unique kinematic constraints was implemented.

4.1. Adhesion Recovery

One way to increase the robustness of Waalbot II's climbing ability is to introduce adhesion sensing and recovery,

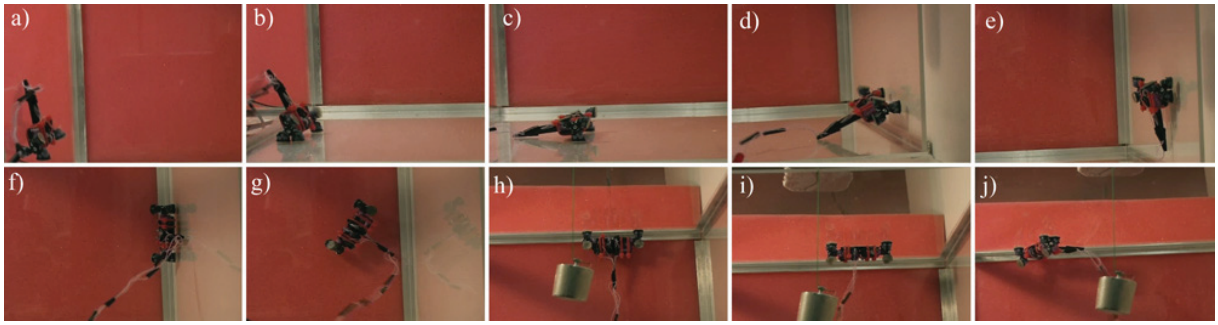

Fig. 14. Small-scale Waalbot climbing inside an acrylic cube with 30 cm sides demonstrating: (a) climbing down a wall; (b) transitioning from a wall to the floor; (c) crawling across the floor; d) floor-to-wall transition; (e) vertical wall climbing; (f) wall-to-wall transition; (g) steering on a wall; (h) wall-to-ceiling transition; (i) inverted steering; (j) inverted climbing.

which will allow the robot to regain adhesion lost due to a misstep, or contaminated fibers. Animals that are skilled at climbing smooth vertical surfaces are capable of sensing how well they are adhered to the surface. For example, if the gecko senses loss in adhesion in the front feet, it will use its tail to counteract the pitchback moment and regain adhesion (Jusufi et al. 2008). Our goal was not to mimic the actions of the animals, but to utilize the principles behind their robust climbing abilities. Therefore, adhesion sensing was implemented on Waalbot using force sensors on each tail, which directly measures the adhesive force of the corresponding foot through the quasi-static force transfer equations presented in Murphy and Sitti (2007).

A control scheme was implemented such that when the force of either foot dropped below a certain threshold value the system began an adhesion recovery motion. From experimental results, it is shown that the adhesion recovery is effective and leads to a more robust climbing system. The recovery system takes the tail force as the input and compares it to an empirically defined threshold force, which can be obtained by running experiments on the desired climbing surface. If the tail force is lower than the safety threshold, the system initiates a rocking maneuver, which will be presented in detail. After the recovery, the robot continues to climb normally until the tail force drops below the threshold again when the rocking maneuver is again initiated.

4.1.1. Adhesion Sensor Selection Adding force sensing to the footpads of the robot would be a challenging task due difficulties of adding instrumentation to the six feet which are subject to continuous rotation of the leg mechanisms. Instead, a force sensor at the end of each of the robot's tails was added. Only two sensors are required to capture the adhesion information about the force transfer of all of the feet, and the tails are more easily instrumented due to their proximity to the electronics and their static configuration. These sensors are able to capture the same force information as footpad sensors would because the tail is used as a support to help detach the feet during stepping. During the force transfer from the rear feet to the front feet, the forces on the tails are directly proportional to the pull-off force of the detaching foot (Murphy and Sitti 2007). If the adhesion force is as strong, or stronger than the gravity force, the adhesion can be measured at any surface orientation, since the robot always uses the tail to transfer forces while taking a step. The relationship can be obtained by solving for the tail force as a function of other known parameters, such as

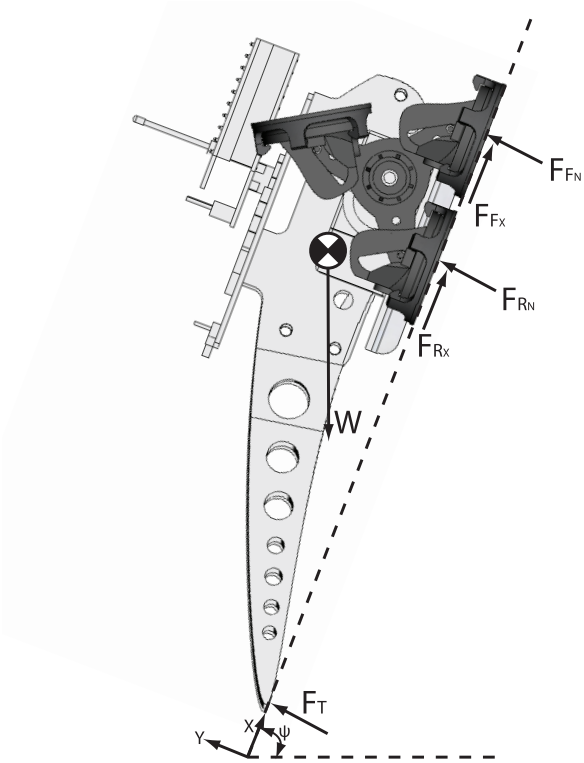

Fig. 15. Free body diagram showing the forces present during a forward step on a surface at angle ψ where the front foot is pressed against the surface and the rear foot is being peeled. F_{RX} and F_{FX} are the rear and front forces, respectively, in the X direction. F_{RN} and F_{FN} are the rear and front forces, respectively, in the normal ,Y, direction. F_T is the tail force, while W is the weight of the robot acting on the center of gravity.

robot weight and geometry, using Figure 15 and assuming negligible tail friction as

$$F_{FY} = \frac{F_T[L + \frac{d_{\text{step}}}{2}] + W\cos(\Psi)[\frac{d_{\text{step}}}{2} - L_{xcg}] + W\sin(\Psi)[-2L_{ycg}]}{d_{\text{step}}} \quad (2)$$

where F_{FY} is the normal force on the front food, F_T is the tail force, d_{step} is the distance between the ankles of two feet, W is the robot weight, Ψ is the climbing surface angle, and L_{xcg} and L_{ycg} are the distances from the center of gravity, where the weight acts, to the center of the servo horn and the climbing surface, respectively. To have a high safety factor, the gravity component of the tail force is minimized by having the robot body close to the wall, which means a small value of L_{ycg}. This equation is only accurate for climbing up or down a surface at any orientation. If the robot climbs sideways, the equation would need to be modified to reflect the imbalance in the distribution of the weight between the tails.

Piezoresistive force sensors (0.2" Interlink FSR) were chosen, due to their small mass and size, and ease of integration. These sensors were added to the electronics in a voltage divider configuration. The resistor value was selected to optimize the range of the output voltage from the sensor over the force range that the robot is able to produce at the tail (0–4 N), determined using the value of the maximum torque output from the servo and the moment arm between the servo and the tip of the tail. Tests were then run using a load cell and a motorized stage with applied force values from 0 to 4 N and the sensor was characterized for linearity, repeatability, and drift. Although the response was nonlinear, the sensor had acceptable repeatability, and negligible drift.

4.1.2. Adhesion Level Sensing and Recovery The tail force sensors were integrated into Waalbot II, and software was written to record and report the maximum tail force sensed during each step. The maximum tail force occurs right at pull-off from the surface; however, this is a difficult event to catch as it is rapid. To increase the chances of capturing the most accurate reading, the force sensors are continuously polled, at the limit of the microprocessor and program code, and the maximum of the set of readings is taken as the maximum tail force. An instrumented Waalbot II was tested with magnetic footpads on a metal surface to investigate the reliability of the adhesion sensing. The adhesion from the magnetic feet was observed to remain constant over many robot steps, indicating that the force sensors functioned as intended.

To regain adhesion, Waalbot II brings two feet on the side where adhesion was lost into contact with the surface, and then commands the motors forward and backward at a constant torque value without allowing either foot to completely detach. We propose that pressing back and forth between the attached feet, using the same force to press down on the feet each time, engages increasingly more fibers as they are able to avoid dirt particles and thus a higher effective contact area is gained, which increases the adhesion (Figure 16).

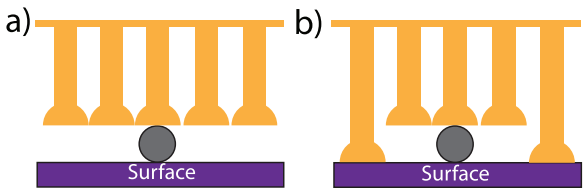

Fig. 16. Possible mechanism of adhesion increase during rocking motion: (a) illustration showing a piece of dirt that inhibits surrounding fibers from engaging with the surface; (b) more fibers can engage with the surface when repeatedly loaded and unloaded during rocking maneuvers.

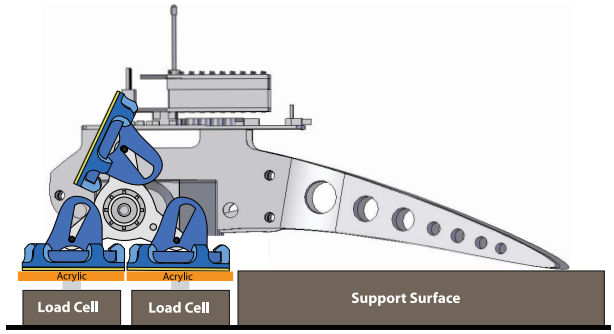

Fig. 17. Illustration showing the setup to examine the effect of a rocking motion using constant preload.

The rocking motion applies normal forces to preload the front and rear feet without letting the other foot detach from the surface by alternating the direction of the motor and only allowing a small rotation of the leg. To test the hypothesis that rocking at a constant torque setting will increase the adhesion, an experiment was run. The robot, with fibrillar adhesive footpads, was placed on a surface with a 10 lb load cell (MLP-10; Transducer Techniques Inc.) under each foot on one side (Figure 17). The other side of the robot and both tails were supported by a stationary surface. The voltage readings from both of the load cells, which represent the force on the front and rear foots separately, were recorded through a data acquisition board (NI PCI-6259; National Instruments). The robot then performed the rocking maneuver and the forces were recorded. As seen in Figure 18, the adhesive force increases with an increase in the number of rocking motions.

To test the adhesion threshold value *in situ*, the robot was commanded to climb vertically on an acrylic surface that had surface imperfections, and forces were recorded until the robot fell from the surface. The adhesion values recorded before the robot detached from the surface were taken as the safety threshold for the adhesion and this was

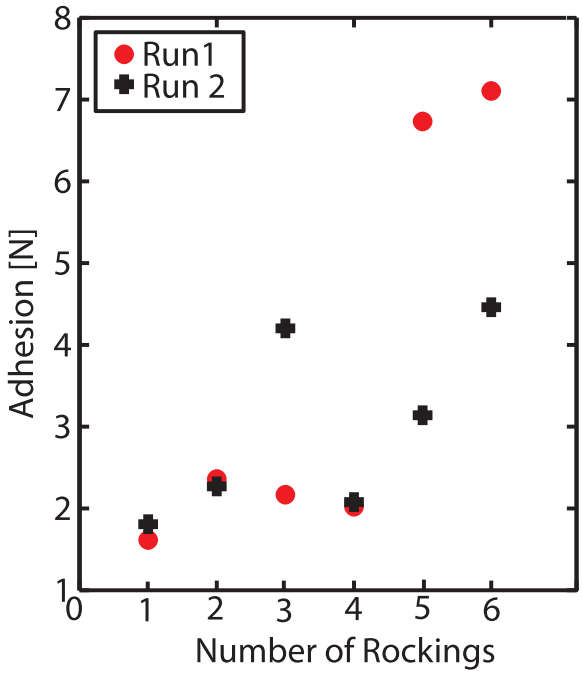

Fig. 18. Experimental results showing the increase in adhesion when the number of rocking maneuvers is increased, when rocking using a constant preload.

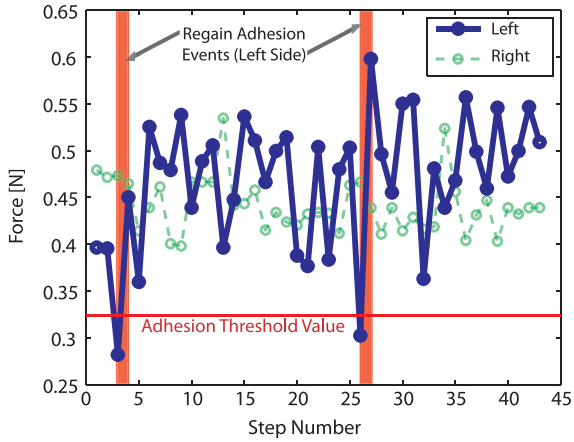

Fig. 19. Plot showing the force on the feet over many steps as well as the increase in adhesion due to regain adhesion events. When the force on the tail sensor drops below 0.325 N, the adhesion regain event is triggered and the adhesion then increased on the subsequent step.

empirically set to be 0.325 N. The threshold value is dependent and needs to be updated if the environmental conditions change, which includes continued degradation of the fibers. Increasing the life-time of the adhesive and using more accurate force sensors would decrease the sensitivity of the threshold value.

The robot was programmed to sense when the adhesion force dropped below the safety threshold and to then perform an adhesion regaining action. The recovery motion ceases once five rocking cycles have been completed, which experiments show to be a sufficient adhesion recovery to continue climbing (Figure 18). As seen in Figure 19, the adhesion recovery action begins once the force sensor value drops below the threshold, 0.325 N. After the adhesion recovery event, the robot regains the adhesion during the subsequent steps (Figure 19).

4.2. Motion Planning

There is significant interest in utilizing climbing robots for inspection and surveillance applications. In motivating the design of a planning algorithm, we considered Waalbot II's use in a man-made environment with the benefit of external hardware for environment modeling and robot localization. Our implementation assumes the use of VICON motion capture cameras for modeling and localization tasks as presented by Halaas et al. (2009) and Saad et al. (2009). The critical aspect of the system is that it generates a tessellated 3D model of the environment and robot pose and location, which are then fed into our algorithm. Our planner begins by decomposing this 3D environment into locally flat 2D regions. We implement a hierarchical algorithm to find a multi-region solution trajectory across the connected locally flat regions. This implementation was developed independently, but is similar to the approach taken by Morisset et al. (2009) and Bretl et al. (2005).

The upper level planner generates a graph of valid configurations along the boundaries between regions or, more conveniently, waypoints. Then, using Euclidean distance heuristics and A* search on the graph, the upper level planner chooses the lowest cost trajectories between waypoints. The trajectories across a single 2D region are then updated by the lower level planner, which functions as a primitive planner, wherein a separate A* algorithm is used to search a discrete state space. The state space is expanded by generating new states of all possible motion primitives from the lowest cost state in the priority queue at each iteration. The upper level planner updates the trajectory costs in its graph according to the lower level planner's actual costs and continues its search, only running the more computationally intensive lower level planner as needed. When the upper level planner has completed its search and found the optimal path it creates a composite trajectory from the multiple lower level planner trajectories, each across a single locally flat 2D region (Figure 20). A video showing a solution trajectory being followed by Waalbot II can be seen in Extension 2. The motion planning is conducted off-board and the motion commands are sent to the robot wirelessly from a controller computer.

5. Conclusion

The final wireless robot prototype demonstrates high agility by performing difficult maneuvers, such as steering with

Table 1. Comparison of Design Aspects and Performance

Design aspect	Waalbot	Waalbot II
Tail design	Single tail	Double tail with body hinge
Adhesive	Flat tacky elastomer	Dry micro-fibrillar adhesive
Electronics	PCB as body (30 g)	Small attached PCB (10 g)
Climbable wall orientations	0 to 110°	Any
Climbable transitions	Floor-to-wall	Floor-to-wall, wall-to-wall, wall-to-ceiling
Climbable surface	Smooth	Smooth or low roughness ($\leq 35\ \mu$m RMS)
Sensing	None	Adhesion and orientation sensing
Foot design	Tabs inside ankle	Tabs outside ankle (closer to wall)
Peeling	None	Passive
Maximum payload	0 g	100 g
Control	Teleoperated	Teleoperated or semi-autonomous
Communication	Receive IR commands	Bi-directional RF

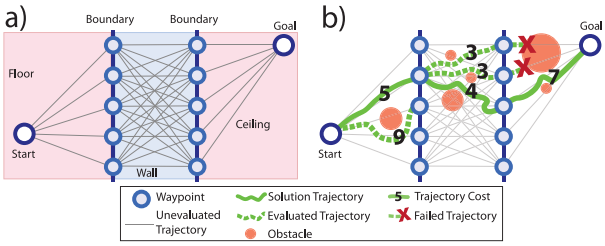

Fig. 20. Overview of the two-level motion planner: (a) waypoints are generated along transitionable plane intersections and connected; (b) trajectories are generated to plan a path between the waypoints. The relative orientations of the wall, floor, and ceiling are arbitrary.

a small turning radius, and transitioning between surfaces of different orientations, including floor-to-wall, wall-to-wall, and wall-to-ceiling transitions, while climbing with dry fibrillar adhesives. Climbing and steering on inverted smooth surfaces, and climbing and steering on non-smooth surfaces, such as wood, have been demonstrated. The new design also exhibited the robot's ability to carry a payload that is more than the bodyweight of the robot. To the authors' knowledge, no other dry-adhesives-based climbing robot can perform sharp turns, plane transitions, and inverted climbing, and climb on non-smooth surfaces.

In this paper, we showed and validated improvements to Waalbot's mechanical design. With the inclusion of fiber footpads, the passive peeling feet were necessary, and they were able to lower power consumption, and increase climbing speed and robot dependability. The new tail design, which included two tails and a passive pin joint, prevented unwanted cross-body movements and can be applied to other climbing robots to increase their reliability. Through an analysis of the scaling equations governing the robot design, an understanding of the robot length and its subsequent ability to carry a payload of a certain mass with a theoretical factor of safety was also explored. The results were then validated by building and testing two different sized Waalbots.

The robot is now capable of obtaining information about its climbing state in the world. The robot is capable of sensing the adhesion force on each of the six feet by using only two force sensors, which are mounted on the tails. From the force sensor data, the robot is then able to regain adhesion lost due to fiber degradation by rocking to be able to continue climbing safely for a prolonged period of time. A two-level motion planner was developed and implemented such that transitions between locally flat regions were identified using the upper level planner and the specific robot trajectory was planned using an A* search. Results show that the robot's trajectories closely match the planned trajectories.

One of the major disadvantages of this robot design is that there is very little redundancy with respect to adhesion failure. To maximize the agility of the robot, increasing its speed and decreasing the turning radius, redundant attachment points were left out of the design. Much of the time, there are only two feet attached to the surface. As the adhesives gather dust and other contaminants, their performance degrades quickly. Therefore, these adhesives are currently not suitable for dirty outdoor environments, walking across indoor floors, or for long-term tasks. Furthermore, the possibility of adhesion failure during a plane transition when improper foot placement occurs is a dangerous flaw for a climbing robot, but could be mitigated by adding additional passive degrees of freedom in the foot.

Future work includes further miniaturization of the robot for improved performance. As the required on-board electronics, such as wireless communications, sensing, and control become available in smaller packages, the robot should be easily scalable, at least to the small-scale (15 g) size of the prototype from Section 3. Other improvements include the ability to walk on dirty ground without contaminating the fiber footpads. Potentially, the robot could flip itself over simply by running the legs in reverse to walk on the

back-sides of its ankles. This improvement would also enable the robot to self-right in the case of a fall where it lands on its back. Further improvements in fiber adhesives would include addressing degradation issues to allow for more reliable adhesion and adding directional adhesion to allow the robot to be even more power efficient in the removal of the feet from the climbing surface. The tail and body design can be further improved to allow the robot to traverse external transitions and thus increase the environmental space in which the robot can operate.

Funding and Acknowledgements

We would like to thank Boeing Corporation for financial contributions to this project.

References

Aksak, B., Murphy, M., and Sitti, M. (2007). Adhesion of biologically inspired vertical and angled polymer microfiber arrays. *Langmuir*, **23**(6): 3322–3332.

Aksak, B., Murphy, M. P., and Sitti, M. (2008). Gecko inspired micro-fibrillar adhesives for wall climbing robots on micro/nanoscale rough surfaces. *IEEE International Conference on Robotics and Automation*, Pasadena, CA, USA, pp. 3058–3063 May 19–23 2008.

Asbeck, A., Dastoor, S., Parness, A., Fullerton, L., Esparza, N., Soto, D., Heyneman, B., and Cutkosky, M. R. (2009). Climbing rough vertical surfaces with hierarchical directional adhesion. *International Conference on Robotics and Automation*, pp. 2675–2680. Kobe, Japan, May 12–17, 2009.

Autumn, K., Hsieh, S. T., Dudek, D. M., Chen, J., Chitaphan, C., and Full, R. J. (2006). Dynamics of geckos running vertically. *Journal of Experimental Biology*, 209(2): 260–272. http://jeb.biologists.org/cgi/content/abstract/209/2/260.

Autumn, K., Liang, Y. A., Hsieh, S. T., Zesch, W., Chan, W. P., Kenny, T. W., Fearing, R., and Full, R. J. (2000). Adhesive force of a single gecko foot-hair. *Nature*, 405: 681–685.

Berengueres, J., Tadakuma, K., Kamoi, T., and Kratz, R. (2007). Compliant distributed magnetic adhesion device for wall climbing. Rome, Italy, April 10-14, 2007. *IEEE International Conference on Robotics and Automation,* 2007, pp. 1256–1261.

Bhushan, B. and Sayer, R. A. (2006). Surface characterization and friction of a bio-inspired reversible adhesive tape. *Microsystem Technologies*,13(1): 71–78.

Bretl, T., Lall, S., Latombe, J.C., &. Rock, S. (2004). Multistep motion planning for a free-climbing robot. Workshop on Algorithmic Foundations of Robotics (WAFR'04), Utrecht, The Netherlands.

Bretl, T., Rock, S., and Latombe, J.-C. (2003). Motion planning for a three-limbed climbing robot in vertical natural terrain. *International Conference on Robotics and Automation*, Taipei, Taiwan, September 14–19, 2003, pp. 2947–2953.

Cacopardo, G., Longo, D., and Muscato, G. (2003). Design of the Alicia3 robot – A modular approach. *6th International Conference on Climbing and Walking Robot*, Catania (Italy), pp. 801-808, 17-19 September 2003.

Daltorio, K. A., Wei, T. E., Horchler, A. D., Southard, L., Wile, G. D., Quinn, R. D., Gorb, S. N., and Ritzmann, R. E. (2009). Mini-whegs tm climbs steep surfaces using insect-inspired attachment mechanisms. *The International Journal of Robotics Research*, 28(2): 285–302.

delCampo, A., Greiner, C., and Arzt, E. (2007). Contact shape controls adhesion of bioinspired fibrillar surfaces. *Langmuir*, **23**(20): 10235–10243.

Fei, Y., Zhao, X., and Wan, J. (2006). Motion analysis of a modular inspection robot with magnetic wheels. *The Sixth World Congress on Intelligent Control and Automation, 2006 (WCICA 2006)*, vol. 2, pp. 8187–8190, Dalian, China, June 21–23, 2006.

Ge, L., Sethi, S., Ci, L., Ajayan, P. M., and Dhinojwala, A. (2007). Carbon nanotube-based synthetic gecko tapes. *Proceedings of the National Academy of Sciences*, **104**(26): 10792–10795.

Grieco, J., Prieto, M., Armada, M., and Gonzalez de Santos, P. (1998). A six-legged climbing robot for high payloads. *Proceedings of the 1998 IEEE International Conference on Control Applications*, vol. 1, pp. 446–450, Trieste, Italy, September 1–4, 1998.

Guan, Y., Jiang, L., and Zhang, X. (2007). Mechanical design and basic analysis of a modular robot with special climbing and manipulation functions. *IEEE International Conference on Robotics and Biomimetics, 2007 (ROBIO 2007)*, pp. 502–507, Sanya, China, December 15-18, 2007.

Halaas, D., Bieniawski, S., Pigg, P., and Vian, J. (2009). Control and management of an indoor, health enabled, heterogenous fleet. *Proceedings 2009 AIAA Infotech@Aerospace Conference*, Seattle, WA, USA, April 6–9, 2009.

Hansen, W. R. and Autumn, K. (2005). Evidence for self-cleaning in gecko setae. *Proceedings of the National Academy of Sciences of the United States of America*, **102**(2): 385–389.

Haynes, G. C. and Rizzi, A. (2006). Gait regulation and feedback on a robotic climbing hexapod. *Proceedings of Robotics: Science and Systems*.

Hirose, S., Nagakubo, A., and Toyama, R. (1991). Machine that can walk and climb on floors, walls and ceilings. *Fifth International Conference on Advanced Robotics, 1991. 'Robots in Unstructured Environments', 91 ICAR*, vol. 1, pp. 753–758, 19 Jun 1991–22 Jun 1991 Pisa , Italy.

Irschick, D. J., Austin, C., Petren, K., Fisher, R. N., Losos, J. B., and Ellers, O. (1996). A comparative analysis of clinging ability among pad-bearing lizards. *Biological Journal of the Linnean Society*, 59: 21–35.

Jeong, H. E., Lee, J.-K., Kim, H. N., Moon, S. H., and Suh, K. Y. (2009). A nontransferring dry adhesive with hierarchical polymer nanohairs. *Proceedings of the National Academy of Sciences*. 106(14): 5639—5644

Jusufi, A., Goldman, D. I., Revzen, S., and Full, R. J. (2008). Active tails enhance arboreal acrobatics in geckos. *Proceedings of the National Academy of Sciences*. 105(11): 4215–4219.

Kalra, L. P., Gu, J., and Meng, M. (2006). A wall climbing robot for oil tank inspection. *IEEE International Conference on Robotics and Biomimetics, 2006 (ROBIO '06)*, pp. 1523–1528, Brussels, Belgium, September 12–14, 2006.

Kim, H., Kim, D., Yang, H., Lee, K., Seo, K., Chang, D., and Kim, J. (2006). A wall climbing robot with vacuum caterpillar wheel system operated by mechanical valve. *International Conference on Climbing and Walking Robots (CLAWAR)*, pp. 28–33.

Kim, S., Asbeck, A. T., Cutkosky, M. R., and Provancher, W. R. (2005). Spinybotii: climbing hard walls with compliant

microspines. Proceedings of the 12th International Conference on Advanced Robotics (ICAR) 18-20 July 2005, Seattle, WA, USA

Kim, S. and Sitti, M. (2006). Biologically inspired polymer microfibers with spatulate tips as repeatable fibrillar adhesives. *Applied Physics Letters*, 89(26): 261911.

Kim, S., Spenko, M., Trujillo, S., Heyneman, B., Santos, D., and Cutkosky, M. R. (2008). Smooth vertical surface climbing with directional adhesion. *IEEE Transactions on Robotics*, 24(1): 65–74.

Lal Tummala, R., Mukherjee, R., Xi, N., Aslam, D., Dulimarta, H., Xiao, J., Minor, M., and Dang, G. (2002). Climbing the walls [robots]. *IEEE Robotics & Automation Magazine*,9(4): 10–19.

Lee, J., Fearing, R. S., and Komvopoulos, K. (2008). Directional adhesion of gecko-inspired angled microfiber arrays. *Applied Physics Letters*, 93(19): 191910.

Linder, S., Wei, E., and Clay, A. (2005). Robotic rock climbing using computer vision and force feedback. *Proceedings of the 2005 IEEE International Conference on Robotics and Automation (ICRA 2005)*, pp. 4685–4690, Barcelona, Spain, April, 2005.

Miyake, T. and Ishihara, H. (2003). Mechanisms and basic properties of window cleaning robot. *Proceedings of IEEE/IASME International Conference on Advanced Intelligent Mechatronics*, vol. 2, pp. 1372–1377, Kobe, Japan, July 20–24, 2003.

Morisset, B., Rusu, R., Sundaresan, A., Hauser, K., Agrawal, M., Latombe, J., and Beetz, M. (2009). Leaving flatland: toward real-time 3d navigation. *IEEE International Conference on Robotics and Automation*, pp. 3786–3793, Kobe, Japan, May 12–17, 2009.

Murphy, M. P., Aksak, B., and Sitti, M. (2007). Adhesion and anisotropic friction enhancements of angled heterogeneous micro-fiber arrays with spherical and spatula tips. *Journal of Adhesion Science and Technology*, 21(12): 1281–1296.

Murphy, M. P., Aksak, B., and Sitti, M. (2009a). Gecko-inspired directional and controllable adhesion. *Small*, 5(2): 170–175.

Murphy, M. P., Kim, S., and Sitti, M. (2009b). Enhanced adhesion by gecko-inspired hierarchical fibrillar adhesives. *ACS Applied Materials & Interfaces*, 1(4): 849–855.

Murphy, M. P. and Sitti, M. (2007). Waalbot: An agile small-scale wall-climbing robot utilizing dry elastomer adhesives. *IEEE/ASME Transactions on Mechatronics*, 12(3): 330–338.

Prahlad, H., Pelrine, R., Stanford, S., Marlow, J., and Kornbluh, R. (2008). Electroadhesive robots – wall climbing robots enabled by a novel, robust, and electrically controllable adhesion technology. *IEEE International Conference on Robotics and Automation, 2008 (ICRA 2008)*, Pasadena, CA, USA, May 19–23, 2008.

Qu, L., Dai, L., Stone, M., Xia, Z., and Wang, Z. L. (2008). Carbon nanotube arrays with strong shear binding-on and easy normal lifting-off. *Science*, 322(5899): 238–242.

Ryu, S., Park, J., Ryew, S., and Choi, H. (2001). Self-contained wall-climbing robot with closed link mechanism. *IEEE/RSJ International Conference on Intelligent Robots and Systems*, 2001, vol. 2, pp. 839–844, Maui, Hawaii, USA, Oct 29 -NOV. 03, 2001.

Saad, E., Vian, J., Clark, G., and Bieniawski, S. (2009). Vehicle swarm rapid prototyping testbed. *Proceedings 2009 AIAA Infotech@Aerospace Conference* 6–9 April 2009, Seattle, Washington.

Saboori, P., Morris, W., Xiao, J., and Sadegh, A. (2007). Aerodynamic analysis of city-climber robots. *IEEE International Conference on Robotics and Biomimetics (ROBIO)*, pp. 1855–1860, December 15-18, 2007, Sanya, China.

Santos, D., Heyneman, B., Kim, S., Esparza, N., and Cutkosky, M. (2008). Gecko-inspired climbing behaviors on vertical and overhanging surfaces. *IEEE International Conference on Robotics and Automation, 2008 (ICRA 2008)*, pp. 1125–1131, Pasadena, CA, USA, May 19–23, 2008.

Santos, D., Spenko, M., Parness, A., Kim, S., and Cutkosky, M. (2007). Directional adhesion for climbing: theoretical and practical considerations. *Journal of Adhesion Science and Technology*, 21: 1317–1341.

Sethi, S., Ge, L., Ci, L., Ajayan, P. M., and Dhinojwala, A. (2008). Gecko-inspired carbon nanotube-based self-cleaning adhesives. *Nano Letters*, 8(3): 822–825.

Shen, W., Gu, J., and Shen, Y. (2005). Proposed wall climbing robot with permanent magnetic tracks for inspecting oil tanks. *IEEE International Conferenceon Mechatronics and Automation*, 2005, vol. 4, pp. 2072–2077, Niagara Falls, Canada • July 2005.

Unver, O., Murphy, M. P., and Sitti, M. (2005). Geckobot and waalbot: Small-scale wall climbing robots. *Infotech@Aerospoace*, Arlington, VA, pp. 1–10.

Unver, O. and Sitti, M. (2009). A miniature ceiling walking robot with flat tacky elastomeric footpads. *International Conference on Robotics and Automation*, pp. 2276–2281, Kobe, Japan, May 12–17, 2009.

Unver, O., Uneri, A., Aydemir, A., and Sitti, M. (2006). Geckobot: a gecko inspired climbing robot using elastomer adhesives. *IEEE International Conference on Robotics and Automation*, vol. 1, pp. 2329–2335, Orlando, Florida - May 2006.

Wang, W., Wang, Y., Wang, K., Zhang, H., and Zhang, J. (2008). Analysis of the kinematics of module climbing caterpillar robots. *IEEE/ASME International Conference on Advanced Intelligent Mechatronics, 2008 (AIM 2008)*, pp. 84–89, July 2–5, 2008, Xi'an, China.

Wanli, L., Xinghua, Q., and Yonggang, Y. (2007). Design and motion analysis of wheel-legged climbing robot. *Chinese Control Conference, 2007 (CCC 2007)*, pp. 149–153, July 26–31, 2007, Zhangjiajie, Hunan, China.

Wu, S., Li, M., Xiao, S., and Li, Y. (2006). A wireless distributed wall climbing robotic system for reconnaissance purpose. *Proceedings of the 2006 IEEE International Conference on Mechatronics and Automation*, pp. 1308–1312, June 25–28, 2006, Luoyang, China.

Xiao, J. and Sadegh, A. (2007). City Climber: A New Generation Wall-climbing Robots in Zhang H (ed): *Climbing & Walking Robots, Towards New Applications*. Vienna, Austria.

Yamamoto, A., Nakashima, T., and Higuchi, T. (2007). Wall climbing mechanisms using electrostatic attraction generated by flexible electrodes. *International Symposium on Micro-NanoMechatronics and Human Science, 2007 (MHS '07)*, pp. 389–394, Nov. 11–Nov. 14, 2007, Nagoya, Japan.

Yan, W., Shuliang, L., Dianguo, X., Yanzheng, Z., Hao, S., and Xueshan, G. (1999). Development and application of wall-climbing robots. *IEEE International Conference on Robotics and Automation*, 1999, vol. 2, pp. 1207–1212, Detroit, Michigan May 1999.

Yano, T., Suwa, T., Murakami, M., and Yamamoto, T. (1997). Development of a semi self-contained wall climbing robot with scanning type suction cups. *Proceedings of the 1997 IEEE/RSJ International Conference on Intelligent Robots and Systems (IROS '97)*, vol. 2, pp. 900–905, September 7–11, 1997 Grenoble, France.

Yuan Qian, Z., zheng Zhao, Y., and Fu, Z. (2006). Development of wall-climbing robots with sliding suction cups. *2006 IEEE/RSJ International Conference on Intelligent Robots and Systems*, pp. 3417–3422, October 9–15, 2006, Beijing, China.

Yurdumakan, B., Raravikar, N. R., Ajayan, P. M., and Dhinojwala, A. (2005). Synthetic gecko foot-hairs from multiwalled carbon nanotubes. *Chemical Communications*, 30: 3799–3801.

Zhao, Y., Tong, T., Delzeit, L., Kashani, A., Meyyappan, M., and Majumdar, A. (2006). Interfacial energy and strength of multiwalled-carbon-nanotube-based dry adhesive. *Journal of Vacuum Science & Technology B*, **24**: 331–335.

Zhu, T., Liu, R., Wang, X. D., and Wang, K. (2006). Principle and application of vibrating suction method. *IEEE International Conference on Robotics and Biomimetics, 2006 (ROBIO '06)*, pp. 491–495, December 17–20, 2006, Kunming, China.

A. Index to Multimedia Extensions

Extension	Type	Description
1	Video	Climbing demonstrations using microfibrillar adhesives
2	Video	Motion planning demonstration